The discrete temporal eigenvalue spectrum of the generalised Hiemenz flow as solution of the Orr-Sommerfeld equation

V. THEOFILIS

Department of Applied Mathematics, University of Twente, Postbus 217, 7500 AE Enschede, the Netherlands

Abstract. A spectral collocation method is used to obtain the solution to the Orr-Sommerfeld stability equation. The accuracy of the method is established by comparing against well documented flows, such as the plane Poiseuille and the Blasius Boundary layers.

The focus is then placed on the generalised Hiemenz flow, an exact solution to the Navier-Stokes equations constituting the base flow at the leading edge of swept cylinders and aerofoils. The spanwise profile of this flow is very similar to that of Blasius but, unlike the latter case, there is no rational approximation leading to the Orr-Sommerfeld equation.

We will show that if, based on experimentally obtained intuition, a nonrational reduction of the full system of linear stability equations is attempted and the resulting Orr-Sommerfeld equation is solved, the linear stability critical Reynolds number is overestimated, as has indeed been done in the past.

However, as shown by recent Direct Numerical Simulation results, the frequency eigenspectrum of instability waves may still be obtained through solution of the Orr-Sommerfeld equation. This fact lends some credibility to the assumption under which the Orr-Sommerfeld equation is obtained insofar as the identification of the frequency regime responsible for linear growth is concerned.

Finally, an argument is presented pointing towards potential directions in the ongoing research for explanation of subcriticality in the leading edge boundary layer.

1. Introduction

The linear stability of a small class of problems of engineering significance may be studied by solution of the Orr-Sommerfeld equation. Best known examples of these are the Blasius Boundary layer and the plane Poiseuille flow. While the plane Poiseuille flow is strictly parallel, in the former case a non-rational argument regarding parallel mean flow has to be invoked, in order for the system of stability equations resulting from substitution of small wave-like perturbations into the Navier-Stokes equations and linearisation about the Blasius profile to be reducible to the Orr-Sommerfeld equation.

The flow at the attachment line forming near the leading edge of swept aerofoils and cylinders, on the other hand, is attractive from a mathematical viewpoint for (at least) two reasons. Firstly, this flow is an exact solution of the Navier-Stokes equations (Hiemenz [1], Schlichting [2]). As a consequence no boundary layer assumption, based on the largeness of Reynolds number, is required and, hence, the search for a critical Reynolds number of this flow is based on a self-consistent theory. Further, the boundary layer set up at the attachment line is strictly parallel, thus significantly simplifying the linear stability analysis compared to the flat plate boundary layer, where the slow growth of the layer has to be taken into account.

For more than a decade now, and stemming from the renewed efforts around Natural Laminar Flow Control, a number of studies of the generalised Hiemenz flow have been performed. Experimentally, Poll undertook detailed investigations [3]–[6] and proposed a

critical Reynolds number value of $R_\theta \approx 235$. Theoretically, Hall et al. [7] and Hall and Malik [8] studied the linear and weakly nonlinear regimes by solution of the eigenvalue problem and Direct Numerical Simulation (DNS). Spalart [9] performed a DNS of instability, transition, turbulence and relaminarisation of this flow. Jiménez et al. [10] also performed a DNS of the linear and nonlinear regimes, while Theofilis [11, 12] studies the eigenvalue problem and performed a DNS in the linear regime.

Despite this activity, open questions still remain, mainly revolving around the existence of subcritical instability and the explanation of the origin of the phenomenon of 'leading edge contamination', namely existence of turbulent flow at the attachment line itself at Reynolds numbers well below critical limits established through linear and weakly nonlinear analyses. In this work, however, we restrict ourselves in scope and, using recent DNS results, turn to the possibility of studying, from an engineering viewpoint, the frequency eigenspectrum of the flow under consideration by reduction of the full stability problem to the Orr-Sommerfeld equation, which can be solved efficiently on a modest present day machine.

There is no rational argument which may lead to such a reduction. However, the experimental observation that this flow is strictly parallel in the spanwise direction might, conceivably, leave some room for questioning the necessity for extraction of physically relevant information on the frequency eigenspectrum from solution of the full eigenvalue problem or, ultimately, from DNS alone.

To address this question, we first solve the Orr-Sommerfeld equation by a spectral decomposition of the perturbation quantities. Ever since its introduction in the early 70s, albeit in a somewhat different form, this solution approach for the eigenvalue problem at hand has been gaining ground compared to the more traditional shooting methods based on finite-differences as will be discussed below. In §2 we present the Orr-Sommerfeld equation and its solution alongside a number of validation results. In §3 the equations governing the base flow and the linear stability of the attachment-line boundary layer are presented. The Orr-Sommerfeld equation of this problem is deduced and solved in a region of interesting wave- and Reynolds numbers. Results are compared with past studies, notably with the theoretical/experimental critical Reynolds numbers, as well as with results of a DNS of this problem. Conclusions are discussed in §4.

2. The Orr-Sommerfeld equation

2.1. Formulation of the problem

The stability equation resulting from substitution of small two-dimensional harmonic perturbations into the incompressible Navier-Stokes equations and linearisation about a parallel mean state is the well-known Orr-Sommerfeld equation (Lin [13]),

$$\frac{\mathrm{i}}{\alpha R}(\phi^{IV} - 2\alpha^2\phi'' + \alpha^4\phi) + (w - c)(\phi'' - \alpha^2\phi) - w''\phi = 0\,. \tag{1}$$

A form $\phi(y)\exp(\mathrm{i}\alpha(x - ct))$ has been assumed for the disturbance stream function with x and y denoting respectively the streamwise and normal coordinates and t time. The (real) wave number associated with the disturbance is denoted by α, the (complex) wave velocity by $c = c_r + \mathrm{i}c_i$, R is the Reynolds number and primes denote differentiation with respect to

the variable in the normal direction. The base velocity around which perturbation develop is denoted by w; if a truly accurate solution of the Orr-Sommerfeld equation is to be expected, an accurate specification of w and its second derivative appearing in (1) has to be provided. The boundary conditions following from the asymptotic form of the equation at the endpoints of the integration domain, $\eta = \pm 1$ and $\eta = 0$, $\eta \to \infty$ for the channel and boundary layer flows respectively, are the vanishing of perturbations and their first derivatives, $\phi = \phi' = 0$.

The parallel flow assumption is strictly valid for the channel case but, of course, only a first approximation for the Blasius boundary layer. In the latter case one proceeds by introducing non-parallel effects corresponding to the slow boundary layer growth and solving the resulting stability equation, with the Orr-Sommerfeld solution as a first approximation. However, in this paper we are concerned with the boundary layer set up by introducing a spanwise component into the classical Hiemenz stagnation point flow; the resulting flow is well known to be strictly parallel.

2.2. A spectral collocation solution method for the Orr-Sommerfeld equation

In the influential paper of Orszag [14] the 'exponential convergence' property of spectral methods was exploited in order to obtain a highly accurate solution of the Orr-Sommerfeld equation resulting from a temporal linear stability analysis of the plane channel boundary layer. From [14] onwards the solution method for the linear stability equations, of which the Orr-Sommerfeld is a specific limit, shifted away from classical finite-difference–shooting techniques towards pseudospectral methods due to a number of factors.

Firstly, the pseudospectral method exhibits exponential convergence; with a modest number of nodes one may obtain, when using collocation methods, an accurate solution that would require at least three times as many finite-difference points as was experienced, for example, by Macaraeg et al. [15] compared to COSAL [16]. Secondly, when using shooting from some prescribed value in the free-stream towards the wall, one has to apply successive orthonormalisation in order to avoid the almost linearly dependent perturbation eigenvectors becoming actually linearly dependent. In an already expensive finite-difference calculation this is an additional undesirable requirement. One may apply the method of 'order-reduction' of van Stijn and van de Vooren [17] in order to prevent the solution vectors from becoming linearly dependent but, still, the resulting system has to be solved on a very fine grid for an accurate solution to be obtained [17]. Finally, the iterative approach required by the shooting technique is based on the provision of a reasonably accurate first estimate, otherwise it may well diverge; such an estimate may not exist when one attacks a new flow problem. Even if a starting point for the calculations does exist, having solved for one (R, α) point, one usually moves incrementally in parameter space using the recently obtained result as a first estimate for the next calculation. Such an approach, aside from being tedious, carries with it the potential of missing modes, purely due to the incremental search.

On the contrary, solution of the generalised eigenvalue problem resulting from a spectral discretisation of (1) yields all the eigenvalues members of both the discrete and the infinite spectrum without the need of shooting or iteration. The typical for spectral methods exponential accuracy is exhibited as the number of nodes is increased. On the negative side of a spectral expansion one might quote its higher cost per typical operation, say matrix inversion, compared to a finite-difference calculation, since the matrices resulting from finite-differencing are sparse, as opposed to those of a spectral discretisation which are full.

It is, however, unlikely that large arrays will be required in this incompressible limit, where all eigenfunctions are smooth functions, free from the multiple critical layers typical in compressible flow stability calculations.

Tshebishev polynomials have invariably been considered as basis functions for the expansion of the rapidly oscillating eigenmodes, and will also be used in this part of this work. However, instead of evaluating derivatives using the standard recurrence relations of Tshebishev polynomials, the Tshebishev derivative matrices will be employed, with appropriate stretching incorporated. The reader is referred to Gottlieb et al. [18], Canuto et al. [23], Zang [19] and Boyd [20] for details on the fundamentals of the method. This (collocation) approach adopted may be seen as being conceptually simpler than the standard method of Orszag [14] in that only the physical space solution is involved. The fundamental basis functions being the same, however, namely Tshebishev polynomials, should result in comparable accuracy for both spectral approaches.

In the case of a Blasius-type boundary layer flow, the calculation domain has to be mapped onto the standard Tshebishev domain through some mapping

$$\eta = \eta(x) ,$$

x being the standard collocation points and the derivative matrices $D_{i,j}^{(m)}$ have to be redefined to incorporate the stretching transformation as

$$\hat{D}_{k,j}^{(1)}(\eta) = \frac{\mathrm{d}x}{\mathrm{d}\eta} D_{k,j}^{(1)}(x) , \tag{2}$$

$$\hat{D}_{k,j}^{(2)}(\eta) = \left(\frac{\mathrm{d}x}{\mathrm{d}\eta}\right)^2 D_{k,j}^{(2)}(x) + \frac{\mathrm{d}^2x}{\mathrm{d}\eta^2} D_{k,j}^{(1)}(x) , \tag{3}$$

$$\hat{D}_{k,j}^{(3)}(\eta) = \left(\frac{\mathrm{d}x}{\mathrm{d}\eta}\right)^3 D_{k,j}^{(3)}(x) + 3\frac{\mathrm{d}^2x}{\mathrm{d}\eta^2}\frac{\mathrm{d}x}{\mathrm{d}\eta} D_{k,j}^{(2)}(x) + \frac{\mathrm{d}^3x}{\mathrm{d}\eta^3} D_{k,j}^{(1)}(x) , \tag{4}$$

$$\begin{aligned}\hat{D}_{k,j}^{(4)}(\eta) = {} & \left(\frac{\mathrm{d}x}{\mathrm{d}\eta}\right)^4 D_{k,j}^{(4)}(x) + 6\frac{\mathrm{d}^2x}{\mathrm{d}\eta^2}\left(\frac{\mathrm{d}x}{\mathrm{d}\eta}\right)^2 D_{k,j}^{(3)}(x) \\ & + 3\left(\frac{\mathrm{d}^2x}{\mathrm{d}\eta^2}\right)^2 D_{k,j}^{(2)}(x) + 4\frac{\mathrm{d}^3x}{\mathrm{d}\eta^3}\frac{\mathrm{d}x}{\mathrm{d}\eta} D_{k,j}^{(2)}(x) + \frac{\mathrm{d}^4x}{\mathrm{d}\eta^4} D_{k,j}^{(1)}(x) .\end{aligned} \tag{5}$$

Derivatives of the interpolating polynomials are then calculated in the standard way with $D_{i,j}^{(m)}$ replaced by $\hat{D}_{i,j}^{(m)}$. The generalised eigenvalue problem

$$\mathscr{A}\phi = c\mathscr{B}\phi , \tag{6}$$

results, where the entries of $\mathscr{A}$ and $\mathscr{B}$, $a_{i,j}$ and $b_{i,j}$ respectively, are given by

$$a_{i,j} = \begin{cases} \hat{D}_{i,j}^{(4)} - 2\alpha^2\hat{D}_{i,j}^{(2)} + \alpha^4 - \mathrm{i}\alpha Rw\hat{D}_{i,j}^{(2)} + \mathrm{i}\alpha^3 Rw + \mathrm{i}\alpha R(\hat{D}_{i,j}^{(2)}w) , & i = j \\ \hat{D}_{i,j}^{(4)} - 2\alpha^2\hat{D}_{i,j}^{(2)} - \mathrm{i}\alpha Rw\hat{D}_{i,j}^{(2)} , & i \neq j \end{cases}$$

and

$$b_{i,j} = \begin{cases} -i\alpha R\hat{D}^{(2)}_{i,j} + i\alpha^3 R\,, & i = j \\ -i\alpha R\hat{D}^{(2)}_{i,j}\,, & i \neq j \end{cases}$$

as dictated by the minimisation of the residuals, while $a_{0,j}$, $a_{1,j}$, $a_{N-1,j}$, $a_{N,j}$ and $b_{0,j}$, $b_{1,j}$, $b_{N-1,j}$, $b_{N,j}$ have to be reserved for the imposition of the boundary conditions associated with the problem. Equation (6) may then be solved using the QZ algorithm (Wilkinson [21]), as implemented in standard libraries (NAG [22]), to obtain the complex eigenvalues c and eigenvectors ϕ.

2.3. Validation Results

2.3.1. Plane Channel flow

Two test cases were considered: The first was the classical example of Orszag [14], while the second was taken from Canuto et al. [23], p. 21. In the first case $\alpha = 1.0$ and the length scale in (1) is taken to be half the channel height. The Reynolds number based on this length is $R = 10\,000$. The eigenvalue spectrum of this problem has been grouped and related to that of Blasius flow by Mack [24]. The second case corresponds to $\alpha = 1.0$, and $R = 7500$ and the unstable mode quoted by [23] is

$$0.24989154 + 0.00223497i\,.$$

We used 64 collocation points along the height of the channel and our results for the first test case, as well as those of References [24] and [14] are presented in Table 1. Alongside the unstable mode, the other members of the A- as well as the least stable modes of the P- and S- families are recovered. Our results for the unstable mode as well as some of the least stable ones for the second test case are presented in Table 2.

In Table 1 we note the agreement, to within at least one part in 10^6, between established results and our calculations, for the most interesting, from a stability analysis viewpoint, marginally stable modes, while the agreement is still acceptable for those which are stronger damped. For the second test case, in Table 2, the power of the method to resolve almost linearly dependent modes, such as the mode pairs (2,3), (5,6) and (7,8) is demonstrated. It is such pairs of modes which dictate the need for successive orthonormalisation if a shooting procedure is employed. The role of round-off error of the specific machine used for the computations has been pointed out in Orszag [14] and we believe that the small discrepancy observed in both cases could be attributed to this case. In Fig. 1 the spatial structure of the unstable eigenfunction pertinent to the second case is presented.[1]

2.3.2. The Blasius Boundary Layer

In the case of this boundary layer, the length scale of (1) is the Blasius viscous length $L = \sqrt{\nu x/U_0}$ with ν the kinematic viscosity, x a dimensional $O(1)$ length and U_0 the free-stream velocity. The Reynolds number appearing in (1) is based on L and may be linked to the displacement thickness Reynolds number R_{δ^*} by

$$R_{\delta^*} = \beta R\,,$$

if use is made of the relationship $\delta^* = \beta L$, between L and the displacement thickness δ^* of the Blasius layer, with $\beta = 1.7207876573$.

Table 1. Eigenvalues of antisymmetric disturbances in plane Poiseuille flow grouped following [14] at $\alpha = 1.0$, $R = 10\,000$.

	Ref 14		Ref 18		Present Results	
Mode	c_r	c_i	c_r	ci	c_r	c_i
P1	0.96464	−0.03519	0.96463092	−0.03516728	0.9646307826	−0.0351674238
P2	0.93635	−0.06325	0.93635178	−0.06325157	0.9363517761	−0.0632515698
P3	0.90608	−0.09131	0.90805633	−0.09131286	0.9080562591	−0.0913129895
P4	0.87976	−0.11937	0.87975570	−0.11937073	0.8797551989	−0.1193702593
P5	0.85145	−0.14743	0.8514494	−0.1474256	0.8514521121	−0.1474240869
P6	0.82314	−0.17548	0.8231370	−0.1754781	0.8231418132	−0.1754876077
P7	0.79482	−0.20353	0.794818	−0.203529	0.7947925329	−0.2035503536
P8	0.76649	−0.23159	0.76649	−0.23159	0.7663827538	−0.2314688563
P9	0.73812	−0.25965	0.73812	−0.25969	0.7384144067	−0.2596525847
P10	0.70887	−0.28769	0.70887	−0.28765	0.7089715600	−0.2883657813
A1	0.23753	0.00374	0.23752649	0.00373967	0.2375269234	0.0037396179
A2	0.19006	−0.18282	0.1900592	−0.1828219	0.1900530904	−0.1828220039
A3	0.34911	−0.12450	0.34910682	−0.12450198	0.3490948677	−0.1245007142
A4	0.36850	−0.23382	0.36850	−0.23882	0.3684933483	−0.2388384640
A5	0.47490	−0.20873	0.474901	−0.208731	0.4749134182	−0.2086595296
A6	0.51292	−0.28663	0.51292	−0.28663	0.5128427147	−0.2866524457
A7	0.58721	−0.26716	0.58721	−0.26716	0.5873295068	−0.2672346830
A8	0.63610	−0.32519			0.6362447738	−0.3255555033
A9	0.68286	−0.30761			0.6819252967	−0.3067262470
S1	0.67759	−0.34373			0.6781150102	−0.3436473011
S2	0.67451	−0.38983			0.6745135784	−0.3898782730
S3	0.67321	−0.43580			0.6731954813	−0.4357935786
S4	0.67232	−0.48326			0.6723222732	−0.4832528233
S5	0.67159	−0.53241			0.6715940833	−0.5324047207
S6	0.67097	−0.58327			0.6709668040	−0.5832706093
S7	0.67043	−0.63588			0.6704297661	−0.6358770132
S8	0.66997	−0.69025			0.6699587838	−0.6902518272
S9	0.66957	−0.74642			0.6695707440	−0.7464151978
S10	0.66923	−0.80439			0.6692276597	−0.8043854236
S11	0.66894	−0.86418			0.6689322590	−0.8641786575
S12	0.66868	−0.92582			0.6686918139	−0.9258131384
S13	0.66846	−0.98932			0.6684769988	−0.9893646836

A number of test cases have been considered for this boundary layer which, compared to that in a channel, has the additional complication of an unbounded integration domain, strictly $y \in [0, \infty]$. Domain truncation using some mapping has to be applied and there has been in the literature some discussion about the optimal choices of the mapping, stemming from the proper imposition of the boundary conditions at infinity [23].

As was already mentioned, the accuracy of any stability calculation depends on an accurate prescription in (1) of the base profile $w(y)$ and its second derivative. Profiles of the Falkner-Skan family may be robustly calculated using standard library routines [22] which yield highly accurate solutions in a matter of CPU-seconds. This solution may then be interpolated onto the appropriate stretched grid using, say, piecewise cubic Hermite interpolation which yields the base profile appearing in (1). Alternatively, one may use spectral methods to obtain the solution of the Falkner-Skan profile directly on the spectral grid as done, for example, by Streett et al. [25] and Theofilis [26]. If the latter approach is followed errors potentially introduced by the interpolation procedure are eliminated.

In view of the minimal cost of the shooting approach we opted for this method of

Table 2. Eigenvalues of plane Poiseuille flow disturbances at $\alpha = 1.0$, $R = 7500$.

Mode	c_r	c_i
1	0.249891534448	0.002235013060
2	0.959154248238	−0.040571466088
3	0.959171831608	−0.040599394590
4	0.300561398268	−0.054281886667
5	0.926447153091	−0.072892770171
6	0.926501929760	−0.072965703905
7	0.893715202808	−0.105199143291
8	0.893823802471	−0.105326116085
9	0.860846340656	−0.137491554022
10	0.861150741577	−0.137679740787
11	0.377135723829	−0.139851152897
12	0.450444042683	−0.150075808167
13	0.828754961491	−0.169166564941
14	0.828299105167	−0.170216739178
15	0.209101125598	−0.195833802223
16	0.798136055470	−0.202320307493
17	0.791997969151	−0.206886485219
18	0.756497204304	−0.207884415984
19	0.568994760513	−0.216141492128
20	0.234354853630	−0.216548100114

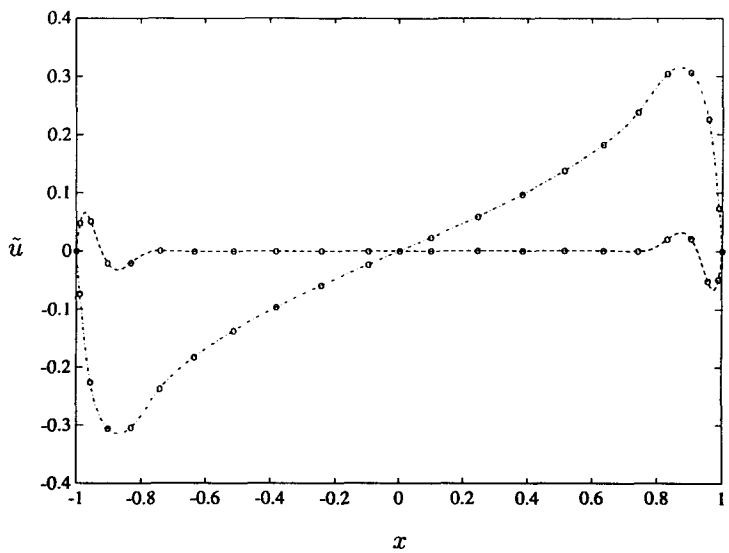

Fig. 1. The spatial structure of the streamwise perturbation velocity eigenfunction $\tilde{u}$ in channel flow at $R = 7500$, $\alpha = 1$. Dashed: $\Re\{\tilde{u}\}$; Dash-dotted: $-\Im\{\tilde{u}\}$.

calculation of the Blasius profile but, instead of using the derivatives as obtained by the library solvers, applied (2)–(5) to the (interpolated) base profile. The result was machine precision agreement between the values for the derivatives yielded by the library subroutine and application of (2)–(5). As expected, this was found to be an essential requirement for the success of any subsequent stability calculation.

The classical test case $\alpha_{\delta^*} = 0.308$, $R_{\delta^*} = 998$ of Mack [24] is considered first. In this case the unstable mode has an eigenvalue [17]

$0.36412129 + 0.00796250\mathrm{i}$.

We solved this case using 64 and 128 collocation points and two mappings between the standard collocation points x_j and the calculation grid η_j, one algebraic

$$\eta_j = l\frac{1-x_j}{1+s+x_j}, \tag{7}$$

with l a length scale and $s = 2l/\eta_\infty$, where η_∞ is the location where the calculation domain for the base flow is truncated, and one exponential. The results obtained using the exponential mapping were indeed more sensitive to the choice of length scale l and hence we employed (7) with $l = \eta_\infty = 50$.

Satisfaction of the boundary condition at infinity required the integration domain to be large enough, this being one of the two most important considerations for an accurate result to be obtained. The other, of course, was a fine enough Tshebishev grid, in order for the discrete descriptions of derivatives (2)–(5) to work well. Having taken both these considerations into account with the choices in resolution made above, we were able to obtain the results of Table 3. The least stable part of the eigenspectrum of the case ($R = 580$, $\alpha = 0.179$) is presented graphically in Fig. 2.

A final validation calculation was performed for the almost incompressible case presented in Table 1 of Macaraeg et al. [15] with the (scaled on boundary layer thickness) parameters assuming the values $R_{\delta^*} = 2200$ and $\alpha_{\delta^*} = 0.2$. The converged result for the unstable mode

Table 3. Discrete eigenvalues of the Blasius boundary layer at $\alpha_{\delta^*} = 0.308$.

Mode	Ref 14		Present results	
#	c_r	c_i	c_r	c_i
			$R = 580$	
1	0.3641	0.0080	0.3641212880	0.0079625034
2	0.2897	−0.2769	0.2897243201	−0.2768738567
3	0.4839	−0.1921	0.4839439094	−0.1920824050
4	0.5572	−0.3653	0.5572212338	−0.3653515279
5	0.6862	−0.3307	0.6862882375	−0.3307860195
			$R = 1000$	
1	0.3383	0.0048	0.3382665514	−0.0048409160
2	0.2408	−0.2391	0.2408009022	−0.2391381114
3	0.4155	−0.1425	0.4155502915	−0.1425429880
4	0.4551	−0.3187	0.4550822377	−0.3187692463
5	0.5773	−0.2730	0.5773537158	−0.2731113135
			$R = 2000$	
1	0.3089	−0.0166	0.3089195489	−0.0165507607
2	0.1918	−0.1961	0.1917774677	−0.1961128264
3	0.3425	−0.0816	0.3425614237	−0.0816631466
4	0.3553	−0.2648	0.3551064431	−0.2651917636
5	0.4651	−0.2079	0.4663228690	−0.2057860642
			$R = 5000$	
1	0.3283	−00.294	0.3284006118	−0.0291462801
2	0.1429	−0.1484	0.1428813040	−0.1483746767
3	0.2172	−0.0456	0.2173307836	−0.0456895940
4	0.2603	−0.2037	0.2649475038	−0.2080391496
5	0.3471	−0.1367	0.3290835917	−0.1292654871

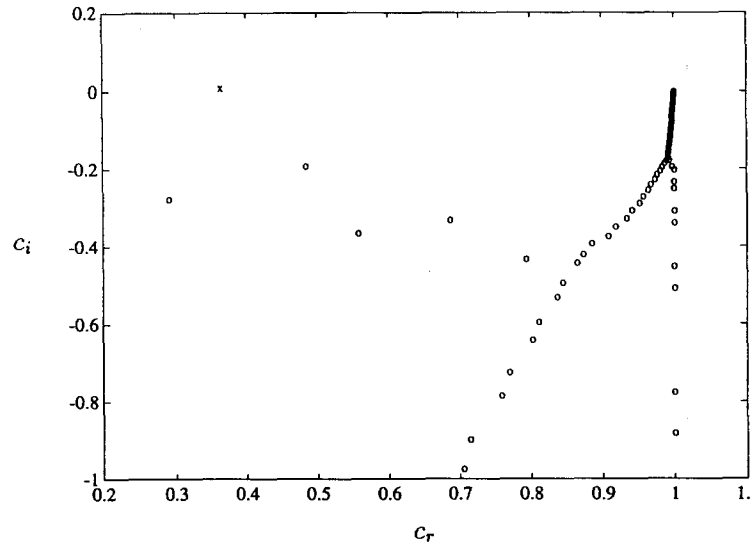

Fig. 2. The eigenvalue spectrum of Blasius flow at $R = 580$, $\alpha = 0.179$. Unstable Mode: '×', Stable Modes: 'O'.

Table 4. Incompressible Unstable Mode at $R = 2200/\beta$, $\alpha = 0.2/\beta$.

	Nodes	$\omega_r \times 10^2$	$\omega_i \times 10^3$
COSAL	1200	5.981375	4.017305
SPECLS	200	5.983575	4.023291
Our calculation	128	5.983654	4.023352

$\omega_r + i\omega_i$ obtained by the standard compressible stability analysis codes COSAL [16] and SPECLS [15] alongside with our calculation is presented in Table 4. It has to be noted that, while both COSAL and SPECLS purity the mode obtained by the global search, i.e. directly solve the appropriate eigenvalue problem and subsequently perform an inverse Rayleigh iteration, our result is that of solution of (6) alone (as a matter of fact the results presented in SPECLS for the global and local search agree to better than eight decimal places). In this respect we will not argue about the correctness of any of the results, our objective being to establish the ability of our solver to capture the interesting modes to within a prescribed tolerance. This seems to be indeed the case, as demonstrated by the results presented for all test-cases, a fact building confidence so as to turn our attention to the subject of investigation next.

3. The generalised Hiemenz boundary layer

3.1. Introduction

In what follows we study the linearly unstable, as well as the marginally stable discrete modes of the Hiemenz boundary layer by means of a DNS of this flow (Theofilis [11, 12]), as well as by solving the (non-rationally obtained) Orr-Sommerfeld equation. Some introductory presentation of the physical problem is in order at this point. For details, the reader is referred, amongst others, to Hall et al. [7] and Theofilis [11].

In order to solve for the base flow over the leading edge of an infinite swept cylinder, we

assume that this face may be treated as locally flat. The oncoming flow outside the boundary layer is taken to be a stagnation-point flow (Schlichting [2]). Taking x to be the chordwise-, y the normal to the attachment line and z the spanwise (along the attachment line) dimensional coordinates, we firstly build a length scale Δ^2 with the aid of the local strain rate of the flow $S = (\mathrm{d}U_e/\mathrm{d}x)_{x=0}$ and the viscosity ν as $\Delta = \sqrt{\nu/S}$. The Reynolds number R of the flow[3] is $R = W_e\Delta/\nu$, W_e being the spanwise velocity component in the far-field and the relation $R_\theta = 0.404R$ links the momentum thickness Reynolds number R_θ to R.
In the absence of any disturbance, the basic flow is taken to be of the form

$$U = Sx\bar{u}(y)\,; \quad V = S\,\Delta\bar{v}(y)\,; \quad W = RS\,\Delta\bar{w}(y) = W_e\bar{w}(y)\,,$$

which, if substituted into the Navier-Stokes equations, leads to the system of Ordinary Differential Equations of the Falkner-Skan family

$$\bar{u} + \bar{v}' = 0\,, \tag{8}$$

$$\bar{v}''' + (\bar{v}')^2 - \bar{v}\bar{v}'' - 1 = 0\,, \tag{9}$$

$$\bar{w}'' - \bar{v}\bar{w}' = 0\,, \tag{10}$$

with boundary conditions

$$\bar{v}(0) = \kappa\,; \qquad \bar{v}'(0) = 0\,; \qquad \bar{v}'(\infty) = -1$$
$$\bar{w}(0) = 0\,; \qquad \bar{w}(\infty) = 1\,,$$

where prime denotes differentiation with respect to the similarity variable $\eta = y/\Delta$ and κ is a non-dimensional parameter used to control suction/blowing in the boundary layer. This reduced form of the Navier-Stokes equations represents a generalisation of the well-known Hiemenz [1] flow in that, in addition to the plane stagnation-point flow, it incorporates a non-zero spanwise velocity component. A straightforward shooting technique is employed to solve this problem in order to obtain the basic flow velocity profile. The result is in excellent agreement with the profiles given, for example, by Rosenhead [27] and Schlichting [2].

Compared to the Blasius boundary layer the spanwise velocity profile of the generalised Hiemenz flow resembles closely that of the (streamwise) Blasius. Significant, from an engineering viewpoint, quantities such as shape factor and skin friction of the Hiemenz flow assume the values $H = 2.54$ and $C_f = 0.461/R_\theta$, as opposed to $H = 2.59$ and $C_f = 0.664/R_\theta$ for Blasius flow. The experimental result for the generalised Hiemenz flow critical momentum thickness Reynolds number, as already mentioned, was given by Poll [4] as $R_\theta \approx 235$.

One assumes that the flow field may be decomposed into base flow quantities (taken to be the generalised Hiemenz flow) and normal modes superimposed upon the base field (see f.e. Hall et al. [7] and Theofilis [11]), i.e.

$$u = Sx\{\bar{u} + R\tilde{u}E\}\,, \tag{11}$$

$$v = W_e\left\{\frac{\bar{v}}{R} + \tilde{v}E\right\}\,, \tag{12}$$

$$w = W_e\{\bar{w} + \tilde{w}E\}\,, \tag{13}$$

with $E = \exp(\mathrm{i}\alpha z - \mathrm{i}\omega t)$, which amounts to studying periodic in the z-direction disturbances

with wavelengths $2\pi/\alpha$. The (non-dimensional) complex frequency ω and wave velocity c are related by $\omega = \alpha c$. The objective now becomes solution of (11)–(13) for the perturbation quantities $(\tilde{u}, \tilde{v}, \tilde{w})$.

3.2. Direct Numerical Simulations

A brief description of the DNS as employed in Theofilis [12] follows. The numerical approach adopted is similar to that of Duck [28], Duck and Burggraf [29], Burggraf and Duck [30] and Theofilis [11] where the reader is referred to for full details.

The unsteady, three-dimensional Navier-Stokes equations expressed using the velocity-vorticity method of Dennis et al. [31] and non-dimensionalised using the boundary layer length scale Δ and the spanwise far-field velocity component W_e to build scales for lengths, velocity, vorticity and time, take the form

$$\nabla^2 \tilde{U} = -\nabla \times \tilde{\zeta} \,, \tag{14}$$

$$\nabla^2 \tilde{\zeta} = R\left\{ \frac{\partial \tilde{\zeta}}{\partial t} + (\tilde{U} \cdot \nabla)\tilde{\zeta} - (\tilde{\zeta} \cdot \nabla)\tilde{U} \right\} , \tag{15}$$

with $\tilde{U}$ and $\tilde{\zeta}$ the velocity and vorticity vectors respectively, t denoting time and R the Reynolds number of the flow defined previously.

Finite-differences on a stretched grid have been utilised in the normal to the wall direction, while the spanwise direction was treated pseudospectrally. The Hiemenz flow (8)–(10) was subtracted away and the equations were marched in time to solve for the perturbation flow quantities. The boundary conditions imposed on perturbations were no slip for the chordwise and spanwise velocity components at the wall and a prespecified forcing function of space and time for the normal velocity component. Boundary conditions for the vorticity have been derived using its definition. In the far field, since we expect all perturbations to decay exponentially, we set all perturbation velocity and vorticity components identically equal to zero (and, of course, considered large enough an integration domain for this condition to be applicable).

For a flow at $R = 750$, $\alpha = 0.3$ a typical result for the wall shear, taken from Theofilis [32], is presented in Fig. 3(a), while the corresponding growth rate is presented in Fig. 3(b). Out of all instability modes excited at the start of the calculation, as time progresses the mode associated with each particular wavenumber emerges.[4] It is by monitoring the convergence of the growth rate of such waves that one deduces information regarding the state in which the flow is found, namely unstable, neutral or stable, as well as quantities such as the frequency of the instability wave.

3.3. Reduction to the Orr-Sommerfeld equation

It is a routine matter in linear stability analyses to substitute the forms (11)–(13) into the full Navier-Stokes equations, subtract the base flow terms (in this case the generalised Hiemenz field, solution of (8)–(10)) and linearise, i.e. neglect quadratic compared to linear in perturbations terms. This procedure, after elimination of the pressure from the equations (a choice dictated by the absence of physical boundary conditions on the pressure perturbation) leads to the following system for the perturbation quantities

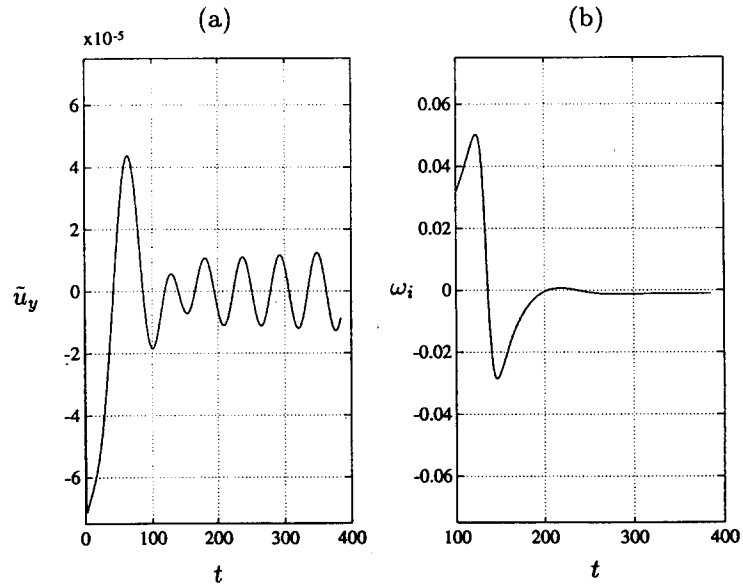

Fig. 3. An instability wave obtained by DNS[32] at $R = 750$, $\alpha = 0.3$: a. perturbation wall shear $\tilde{u}_y$ versus time t, b. growth rate ω_i versus time t.

$$\{\mathcal{D}^2 - \bar{v}\mathcal{D} - \alpha^2 - 2\bar{u} - \mathrm{i}\alpha R\bar{w}\}\tilde{u} - (\mathcal{D}\bar{u})\tilde{v} = -\mathrm{i}\alpha Rc\tilde{u} \tag{16}$$

$$\begin{aligned}\{2(\mathcal{D}\bar{u}) + 2\bar{u}\mathcal{D}\}\tilde{u} + \{\mathcal{D}^4 - \bar{v}\mathcal{D}^3 + [-2\alpha^2 - \mathrm{i}\alpha R\bar{w} - (\mathcal{D}\bar{v})]\mathcal{D}^2 \\ + [\alpha^2\bar{v} + (\mathcal{D}\bar{u})]\mathcal{D} + \alpha^4 + \mathrm{i}\alpha^3 R\bar{w} + \mathrm{i}\alpha R(\mathcal{D}^2\bar{w}) \\ + \alpha^2(\mathcal{D}\bar{v}) + (\mathcal{D}^2\bar{u})\}\tilde{v} = -\mathrm{i}\alpha Rc\{\mathcal{D}^2 - \alpha^2\}\tilde{v}\end{aligned} \tag{17}$$

where $\mathcal{D} = \mathrm{d}/\mathrm{d}\eta$, with $\eta = y/\Delta$. The solution of the full system (16)–(17) has been obtained first by Hall et al. [7] and later in Theofilis [11, 12] (where we termed its solution method a 'time-periodic' scheme). We will not, therefore, be concerned with it for the rest of this work. Instead, we explore the possibility of extracting physically relevant information from a subset of these equations based on experimental intuition rather than mathematical rigour. It should be noted that the solution method for the Orr-Sommerfeld equation presented in §2.2 may be applied to solve the system (16)–(17). However, having to deal with two equations in this case compared to the single Orr-Sommerfeld, and given the cost of the QZ algorithm, it is expected that solving (16)–(17) will be about an order of magnitude more expensive per (R, α) node than the solution of the Orr-Sommerfeld equation for the same number of Tshebishev nodes.

It has been experimentally observed ([4, 6, 7]) that the flow at the attachment line itself is strictly parallel although immediately off the attachment line, of course, it encounters a region of strong acceleration in the streamwise direction. It may therefore seem plausible, from a physical standpoint, to neglect in (16)–(17) all the terms associated with the base flow in the chordwise and normal to the wall directions, $\bar{u}$ and $\bar{v}$ respectively, and thus to keep only terms related to the (predominant) spanwise direction z, namely the spanwise velocity component $\bar{w}$ and its derivatives (which, of course, are related to $\bar{u}$ and $\bar{v}$ through the generalised Hiemenz flow system (8)–(10)). This simplifies (17) to

$$\{\{\mathscr{D}^2-\alpha^2+\mathrm{i}\alpha Rc\}\{\mathscr{D}^2-\alpha^2\}-\mathrm{i}\alpha R\bar{w}\{\mathscr{D}^2-\alpha^2\}+\mathrm{i}\alpha R(\mathscr{D}^2\bar{w})\}\tilde{v}=0\,, \tag{18}$$

which is the Orr-Sommerfeld equation (1). The solution of this equation will be our concern for the rest of this work. Such a simplification, if yielding physically acceptable results, would result, as already mentioned, in significant savings in a day-to-day routine engineering calculation compared to the solution of the full system (16)–(17) or, even more so, compared to the cost of a DNS of this problem [11].

On the other hand, a study of the eigenvalue spectrum is justified in its own right, since it potentially contains the information required for identification of the dangerous, from a stability viewpoint, modes causing transition. We therefore embark upon mapping the region of interest, where transition initiated by small-amplitude disturbances is known to take place, employing the DNS outlined in §3.2 and comparing the results for the frequencies of the unstable modes to those obtained by solution of (18).

3.4. Results

Results for Reynolds numbers in both the stable and unstable flow regimes have been obtained by DNS and the frequencies ($f=1/T$) for the instability waves corresponding to wavenumber values about the neutral loop are presented in Table 5.[5] The inadequacy of the Orr-Sommerfeld equation to predict the critical for instability Reynolds number is known to manifest itself at Reynolds numbers near the tip of the (experimental and DNS) neutral loop $R\approx 585$. It is also expected, and may be observed in the results of Table 5, that solution of (18) is likely to distort the physical picture near Branch I.

However, even on a quantitative level, the error in the frequencies predicted by the Direct Simulation and solution of (18) is well within engineering tolerance and diminishes as Branch II is approached. Far from lending credibility to the unphysical assumptions under which (18) was derived, this agreement implies that one need not resort to expensive simulations alone for the description of the eigenspectrum of frequency of the least stable mode.

A more stringent and physically more interesting test to which results yielded by the model equation (18) may be subjected is the ability of (18) to deliver the crucial, from an engineering point of view, result of a critical for the destabilisation of the attachment line Reynolds number. Using similar assumptions to those we used in the derivation of (18) Poll [3] quoted a critical momentum thickness Reynolds number $R_\theta\approx 270$, a value which was later, experimentally by Poll ([4] and [5]) and theoretically by Hall et al. [7], updated to $R_\theta\approx 235$. The extent to which the neglect of the streamwise and normal velocity components destroyed the physical picture was thus established.

Our result for R_{crit} will follow from a systematic study of the (R,α) region in which linear instability is observed to occur. We solved (18) in (R,α) space between $R=525$ (a choice dictated by the subcriticality reported by Hall and Malik [8]) and $R=1000$. The critical Reynolds number value obtained by linear interpolation between the R values where c_i changes sign is presented in Table 6, alongside the respective frequency (obtained by a similar procedure). This information is also presented alongside the DNS result in Fig. 4. It may be readily observed that the region considered contains the lowest Reynolds number where the change of sign in c_i occurs, $R=666.81$; the value of the critical Reynolds number predicted by solution of (18) may be estimated by these results as being $R\approx 660$. The critical R_θ calculated using this value is $R_\theta\approx 267$, in very good agreement with that obtained by Poll [3], who used similar assumptions. As has already been mentioned, this value has been

Table 5. Comparison between DNS and OS results for the wave period $T = 2\pi/\alpha c_r$ of the least stable waves.

R	α	$(c_r)_{DNS}$	$(T)_{DNS}$	$(c_r)_{OS}$	$(T)_{OS}$
600	0.175	0.358209	100.23	0.348260	103.10
600	0.200	0.362000	86.78	0.357404	87.90
600	0.225	0.368971	75.68	0.365556	76.39
600	0.250	0.375310	66.96	0.379108	66.29
600	0.275	0.380939	59.98	0.379117	60.27
600	0.300	0.386006	54.26	0.384653	54.45
600	0.325	0.390407	49.52	0.389426	49.64
600	0.350	0.394287	45.53	0.393465	45.63
700	0.175	0.349079	102.85	0.341231	105.22
700	0.200	0.353714	88.82	0.350002	89.76
700	0.225	0.360768	77.40	0.357854	78.04
700	0.250	0.366946	68.49	0.364827	68.89
700	0.275	0.372541	61.33	0.370967	61.59
700	0.300	0.377520	55.48	0.376317	55.66
700	0.325	0.381800	50.64	0.380904	50.76
700	0.350	0.385549	46.56	0.384746	46.66
800	0.175	0.344468	104.23	0.333786	107.57
800	0.200	0.346716	90.61	0.345800	90.85
800	0.225	0.353082	79.09	0.351425	79.46
800	0.250	0.359965	69.82	0.356829	70.43
800	0.275	0.365333	62.54	0.364413	62.70
800	0.300	0.370231	56.57	0.369962	56.61
800	0.325	0.374450	51.63	0.372109	51.96
800	0.350	0.377936	47.50	0.378758	47.40
900	0.175	0.337941	106.24	0.327621	109.59
900	0.200	0.340759	92.19	0.340933	92.15
900	0.225	0.347424	80.38	0.345001	80.94
900	0.250	0.353952	71.01	0.351958	71.41
900	0.275	0.359047	63.63	0.358326	63.76
900	0.300	0.363983	57.54	0.364645	57.44
900	0.325	0.368112	52.52	0.367104	52.66
900	0.350	0.371491	48.32	0.370239	48.49
1000	0.175	0.335362	107.06	0.323071	111.13
1000	0.200	0.338753	92.74	0.331946	94.64
1000	0.225	0.344289	81.11	0.340515	82.01
1000	0.250	0.351016	71.60	0.346607	72.51
1000	0.275	0.356331	64.12	0.354327	64.48
1000	0.300	0.361601	57.92	0.358742	58.38
1000	0.325	0.362514	53.33	0.361726	53.45
1000	0.350	0.366292	49.01	0.365224	49.15

Table 6. The critical Reynolds number predicted by solution of (18).

α	R_{crit}	c_r
0.250	698.05	0.364971
0.275	666.81	0.373526
0.300	666.81	0.373526
0.325	683.97	0.375013
0.350	685.84	0.373882

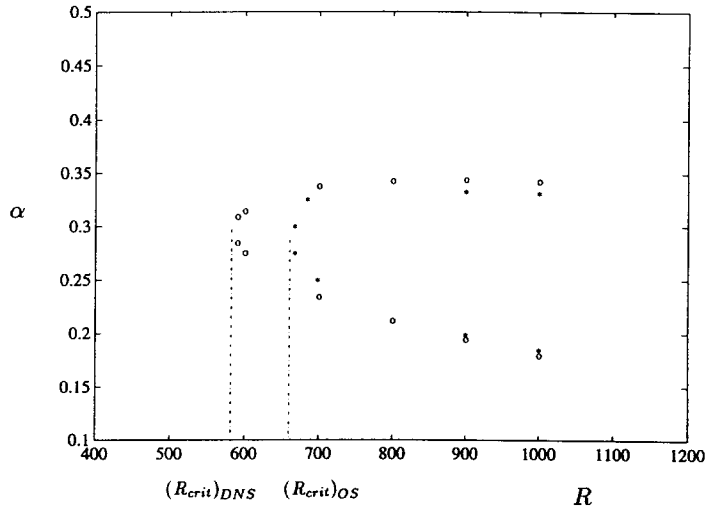

Fig. 4. The (R, α) region considered: 'O': DNS neutral loop; '*': tip of the OS neutral loop; also denoted the critical Reynolds numbers obtained by the two approaches.

updated in [4, 5] and [7], with consistent results having been obtained in the linear regime by Spalart [9], Jiménez et al. [10] and Theofilis ([11], [12] and this work) leaving little doubt that solution of (18) overestimates this physical quantity.

To further substantiate this claim, a set of runs are performed, using the Orr-Sommerfeld equation (18), at a Reynolds number $R = 640$, between the critical values yielded by the two approaches, namely DNS and OS. The result is presented in graphical form in Fig. 5 and it is immediately to be observed that, on one hand the typical pattern of growth rate dependence on wavenumber emerges, on the other, all growth rates are negative indicating, in the sign convention adopted when deriving (18), stable waves. However, it is well known that, as Reynolds number increases, an increasingly better agreement between the Orr-Sommerfeld

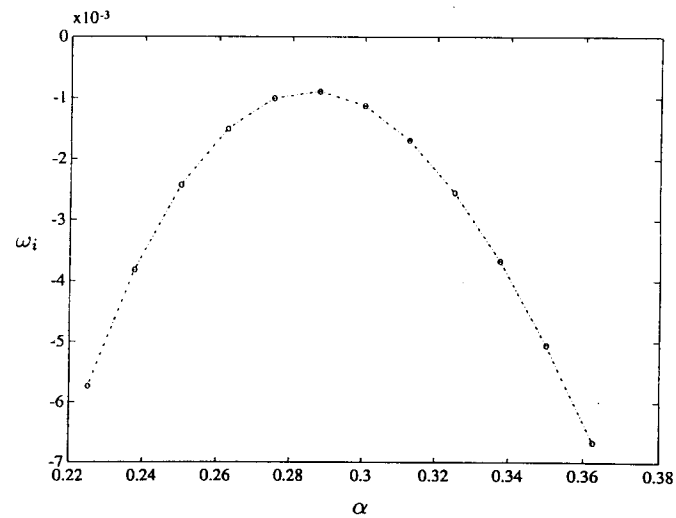

Fig. 5. Growth rate ω_i dependence on wavenumber α at $R = 640$, as solution of the Orr-Sommerfeld equation (18).

result and the experimental and numerical simulation results is obtained (see f.e. Arnal [33]); this point may be supported by the high Reynolds number results of Figure 4 (the Orr-Sommerfeld results obtained by linear interpolation of growth rates at constant Reynolds number). It has been experienced, though, that, as Reynolds number increases, increasingly larger integration times are required before a converged result for the linear growth rates is obtained when DNS is used [12]; even higher Reynolds number results have, therefore, not been obtained in the course of the present work.

Turning our attention now to the frequency spectrum yielded by solution of (18), we see that it may be physically relevant, as demonstrated by the reasonable agreement presented in Table 5. In what follows we will focus upon the behaviour of the three first discrete modes predicted by solution of (18). Naturally, the fact that the frequency of the first mode is reasonably well predicted by (18) does not suggest that all the modes yielded by (18) are physically relevant. Nevertheless, we present our findings here and leave for a later work a detailed study of the spectrum of the full problem, based on solution of the system (16)–(17), as well as a comparison between this spectrum and that of the solution of (18).

The three first modes obtained by mapping the region $R \in (525, 700) - \alpha \in (0.175, 0.35)$ are presented in graphical form in Figs. 6 and 7. What both figures suggest is that, while the frequency of mode 2 is well separated from those of the other two, the frequencies of modes 1 and 3 are very close together, even more so near the critical Reynolds number range where instability is observed. The fact that the first mode remains only marginally stable for quite a long span in R before actually becoming unstable,[6] while mode 3 is not strongly damped either, leaves some room for speculation that in the course of a full Navier-Stokes solution, a large (nonlinear) excitation of such mode pairs may drive an interaction potentially leading to the observed subcriticality. Verification of such an argument will, of course, have to take place in the light of results of the full system (16)–(17) but results obtained in this work may already hint towards a potential direction for future investigation, namely nonlinear interaction of marginally stable linear modes. However, we reserve such a discussion for future work.

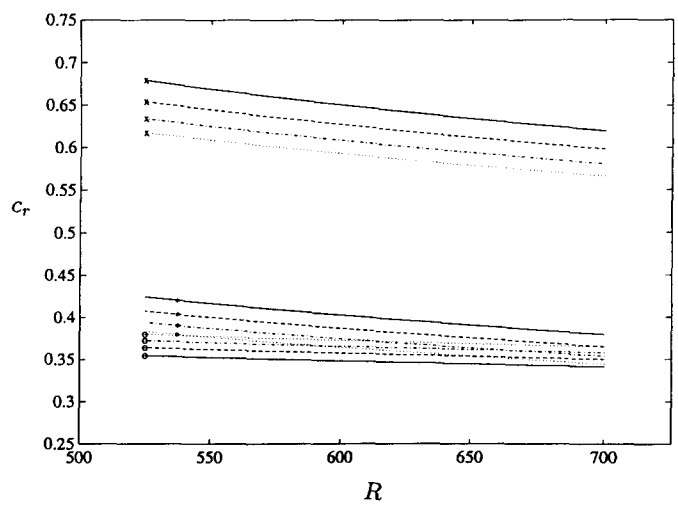

Fig. 6. The first three discrete modes. 'O': Mode 1, '×': Mode 2, '*': Mode 3. Solid: $\alpha = 0.175$, dashed: $\alpha = 0.2$, dash-dotted: $\alpha = 0.225$, dotted: $\alpha = 0.02$.

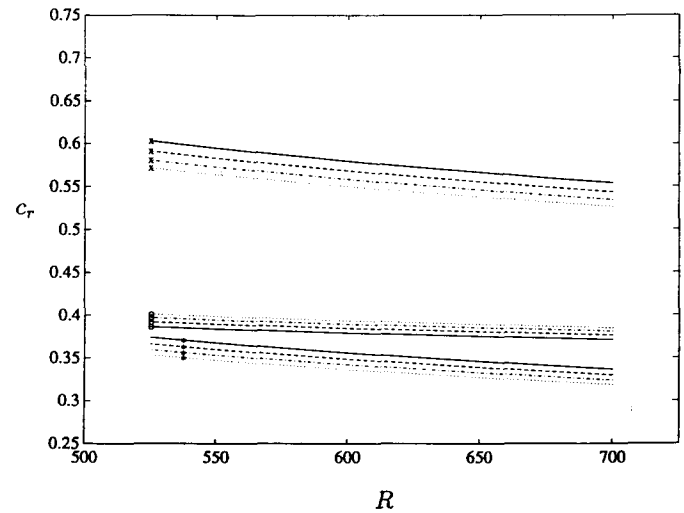

Fig. 7. The first three discrete modes. 'O': Mode 1, '×': Mode 2, '*': Mode 3. Solid: $\alpha = 0.275$, dashed: $\alpha = 0.3$, dash-dotted: $\alpha = 0.325$, dotted: $\alpha = 0.35$.

4. Discussion

Based on the results presented so far we may deduce the following points. First, we obtained an accurate solution to the Orr-Sommerfeld equation, validated on a number of classical test-cases. Further, solving the generalised Hiemenz flow, albeit under a non-rational approximation, yields an interesting result, namely that the frequency eigenspectrum for the most unstable or marginally stable (linear) modes is reasonably well predicted using the solution to the Orr-Sommerfeld equation at a fraction of the cost of the solution of the full system (16)–(17) or a DNS of this flow.

Such a result, of course, is hardly surprising since at a large enough R the spanwise component of this (parallel) flow dominates and the assumptions leading to (18) become more plausible. One would have, however, to resort to the solution of the full system is information regarding R_{crit} is to be obtained, as has been demonstrated by a number of investigations in the past. In any event, the relevance of the linear theory result of R_{crit} in the attachment line is still a subject of investigation.

As a first estimate, however, solution of (18) makes possible, to an engineering accuracy, the identification of the frequency regime in which the linear first mode lies. If physically relevant to the full problem, the picture emerging from a close inspection of the eigenmodes obtained is that there exists a pair of discrete eigenmodes, namely the first and third modes, having similar frequencies while one of them is only marginally stable. Although speculative at this stage, it might be that a nonlinear interaction of these modes carries the potential for destabilisation of a (linearly stable) boundary layer.

Subcriticality in itself, of course, cannot be studied in the framework of linear analyses. A full nonlinear Direct Numerical Simulation of the generalised Hiemenz flow is currently under way (Theofilis [32]), in which modes may be excited selectively and, hence, their potential for destabilisation may be investigated. The solver presented in this work makes it possible to identify the frequency areas to focus upon in the course of such a nonlinear calculation in an accurate and inexpensive way.

Acknowledgements

The author wishes to acknowledge discussions with Professor D.I.A. Poll during the course of the present work. The comments of the Reviewers have improved the quality of the original manuscript and are kindly appreciated. Computations were performed on the Convex C240 of the University of Twente, as well as on the Cray Y-MP/4 of the Stichting Academisch Rekencentrum Amsterdam under the Nationale Computer Faciliteiten grant No. 93/0138.

Notes

1. To be compared with the structure presented in Canuto et al. [23], p. 21, the latter results having been normalised.
2. In view of the assumption of linear dependence of U_e on x in what follows Δ will be defined here as $\Delta = (\nu L/U_e)^{1/2}$, with L an $O(1)$ length and U_e the chordwise velocity component in the free-stream.
3. Customarily denoted by $\bar{R}$.
4. The sign convention for the growth rates adopted in [32] was the opposite of that of the present work; a negative ω_i in [32] actually indicates a growing wave as may be seen in Fig. 3(a).
5. It should be noted that the frequency of the waves presented in Table 5 changes, as is typical in temporal studies, unlike the laboratory environment or spatial numerical investigations where a wave of fixed frequency is inserted in the layer and its (spatial) growth rate monitored in space rather than time.
6. As indicated by monitoring the growth rates of the waves whose frequency is presented in Figures 6 and 7.

References

1. K. Hiemenz, *Dingl. Polytechn. J.* 326 (1911) 321.
2. H. Schlichting, *Boundary Layer Theory*. McGraw-Hill (1979).
3. D.I.A. Poll, *College of Aeronautics* Rep. 7805 (1978).
4. D.I.A. Poll, *The Aeronautical Quart* 30 (1979) 607.
5. D.I.A. Poll, I.U.T.A.M. Symposium on Laminar-Turbulent Transition. Stuttgart, Springer Verlag (1980).
6. D.I.A. Poll, *The Aeronautical Quart.* 34 (1983) 1.
7. P. Hall, M.R. Malik and D.I.A. Poll, *NASA CR-172504* (1984).
8. P. Hall and M.R. Malik, *J. Fluid Mech.* 163 (1986) 257.
9. P.R. Spalart, *AGARD CP-438* (1988) 1–5.
10. J. Jiménez, C. Martel, J.C. Agüi and J.A. Zufiria, *ETSIA* MF-903 (1990).
11. V. Theofilis, Ph.D. Thesis, Dept. of Aeronautical Engineering, University of Manchester (1991).
12. V. Theofilis, *Int. J. Numer. Methods Fluids* 16 (1993) 153.
13. C.C. Lin, *The Theory of Hydrodynamic Stability*, CUP (1955).
14. S.A. Orszag, *J. Fluid Mech.* 50 (1971) 689.
15. M.G. Macaraeg, C.L. Street and M.Y. Hussaini, *NASA TP-2858* (1988).
16. M.R. Malik, *NASA-CR-165952* (1982).
17. Th.L. van Stijn and A.I. van de Vooren, *J. Eng. Math.* 14 (1980) 17.
18. D. Gottlieb, M.Y. Hussaini and S.A. Orszag, in *Spectral Methods for Partial Differential Equations*. (eds. Voigt, R.G. Gottlieb, D. and Hussaini, M.Y.), SIAM Philadelphia, p. 1 (1984).
19. T.A. Zang, *CFD Lecture Series 89-04*. Von Karman Institute for Fluid Dynamics, Brussels (1989).
20. J.P. Boyd, *Chebyshev and Fourier Spectral Methods*. Lecture Notes in Engineering 49, Springer (1989).
21. J.H. Wilkinson, *The algebraic Eigenvalue Problem*. Clarendon (1965).
22. Numerical Algorithms Group, *Mark 15* (1992).
23. C. Canuto, M.Y. Hussaini, A. Quarteroni and T.A. Zang, *Spectral Methods in Fluid Dynamics*. Springer (1988).
24. L.M. Mack, *J. Fluid Mech.* 73 (1976) 497.
25. C.L. Street, T.A. Zang and M.Y. Hussaini, *AIAA Pap. No. 84-0170* (1984).
26. V. Theofilis, Master Class Lecture Notes. *Mathematics Research Institute*, the Netherlands (1993).

27. L. Rosenhead, *Laminar Boundary Layers*. Oxford University Press (1963).
28. P.W. Duck, *J. Fluid Mech.* 160 (1985) 465.
29. P.W. Duck and O.R. Burggraf, *J. Fluid Mech.* 162 (1986) 1.
30. O.R. Burggraf and P.W. Duck, in *Numerical and Physical Aspects of Aerodynamical Flows*. (T. Cebeci ed.), Springer Verlag NY. (1981) 195.
31. S.C.R. Dennis, D.B. Ingham and R.N. Cook, *J. Comp. Phys.* 33 (1979) 325.
32. V. Theofilis, *On subcritical instability of the attachment line boundary layer*. Submitted to *J. Fluid Mech.*
33. D. Arnal, *AGARD Rep. 793*, Von Karman Institute for Fluid Dynamics. Brussels (1993).